TIME-DEPENDENT NONLINEAR THEORY AND NU-MERICAL SIMULATION OF 94 GHz COMPLEX CAVITY GYROTRON

J.-J. Ma[*], X.-F. Zhu, X.-L. Jin, Y.-L. Hu, Z.-H. Yang, J.-Q. Li, and B. Li

National Key Laboratory of Science and Technology on Vacuum Electronics, University of Electronic Science and Technology of China, Chengdu 610054, China

Abstract—A time-dependent nonlinear theory for complex cavity gyrotron is presented in this paper. The theory includes generalized telegrapher's equations and electron motion equations, which are deduced in detail. A calculation code for the self-consistent nonlinear beam-wave interaction is developed based on the presented theory. Using the code, a 94 GHz complex cavity gyrotron operating in TE_{021}–TE_{031} modes is thoroughly studied. Numerical results show that an output power of 180 kW, about 36% efficiency is achieved with a 50 kV, 10 A electron beam at a focused magnetic field of 1.78 T and a beam velocity ratio of 1.65. The results from MAGIC simulation are also given and an output power of 192 kW, 38.4% efficiency is obtained This tells the agreement with these two simulation codes.

1. INTRODUCTION

In millimeter-wave frequency range, the high-power gyrotrons are needed in many applications, e.g., long range radars, electron cyclotron resonance heating of plasma, industrial heating, material processing [1, 2]. As the frequency increases, the gyrotrons encounter mode competition, output radiation mode content, heat wall loading, output power and efficiency increasing problems and need strong magnetic field at the fundamental cyclotron frequency, which makes the magnet heavy and difficult to achieve. The high order harmonic complex-cavity gyrotron with gradual transition has the advantage of overcoming mode competition and enhancing interaction efficiency.

Complex cavities for a gyrotron were proposed by Pavelyev and Tsimring [3] and first practical studies were published by Gaponov et al. [4]. Realization of a stable and high efficient gyrotrons for controlled fusion research was reported in [5]. Coupled cavities with mode conversion in gyrotrons [6, 7] had confirmed the effectiveness of the method of mode selection considered and allowed for an increase in output power and efficiency. Complex cavities were comprised of a set of circular open resonators that supported TE_{mn} modes with different n and equal eigenfrequencies of modes [8].

Vacuum electron devices are based on the interaction between an electron beam and the electromagnetic fields. Modeling and simulation of these devices became a key element in their development [9]. In recent years, there has been significant progress in time-dependent numerical simulations. There are several working codes in which the fields are calculated using the finite-difference time-domain (FDTD) scheme, and the particles are described by the particle-in-cell (PIC) scheme such as MAGIC [10], MAFIA and ARGUS. These codes could be used to simulate and design vacuum electron devices. However, most FDTD-PIC codes need small time for advancement of the FDTD scheme compared with the wave period. Accordingly, the code must be run for a relatively large number of time steps to get to steady state. Furthermore, the spatial resolution usually requires storage of field value on very large matrices. As a direct result, these codes require extensive computing resources. Therefore, there is still a need for accurate and fast design tools for electron-beam devices.

In the past few decades, several theories and codes of gyrotrons have been developed, which include the time-dependent theory derived in [11, 12], linear theory in [13], self-consistent theory in [14]. The simulation code MAGY developed at University of Maryland and Naval Research Laboratory, which is a time-dependent code for simulation of slow and fast microwave sources, is an example of a hybrid code [15]. The code has been used effectively, primarily for the design and simulation of gyro-devices. A hybrid code is a different approach which prepares a highly specialized code [16–18] by incorporating restricting assumptions concerning the physics involved. Such codes require modest computational resources at the price of the restricting model.

In this paper, a self-consistent, time-dependent nonlinear theory is obtained, which is based on a reduced description of the electromagnetic fields and the electron beam. A 94 GHz second harmonic complex cavity gyrotron is simulated to test and verify the nonlinear theory, and the effects of the parameters on the output power and efficiency are stressed to find the optimum parameters of the

complex cavity gyrotron. This is a preliminary study for the complex cavity gyrotron. The paper is organized as follows. In Section 2, the time-dependent nonlinear theory for the complex cavity gyrotron is presented and the generalized telegrapher's equations and the electron motion equations are described. At the same time, the numerical method and initial conditions on the nonlinear theory are simply introduced. Computational results obtained by the developed self-consistent nonlinear code and MAGIC code are discussed in Section 3. Conclusions are given in Section 4.

2. TIME-DEPENDENT NONLINEAR THEORY MODEL

The time-dependent nonlinear theory model includes a time-dependent description of the electromagnetic fields and a self-consistent analysis between the fields and electrons. The theory uses the generalized telegrapher's equations to represent the electromagnetic fields. The equations of electron motion are described in the framework of the guiding-center approximation. When all the trajectories are calculated to update current source, the current source is prepared and the electromagnetic fields are recalculated. This completes the description of the self-consistent beam-wave interaction.

The generalized telegrapher's equations are derived as follows. Firstly, the electromagnetic fields are separated into transverse and longitudinal parts, that is

$$\vec{E}\left(\vec{r},t\right) = \mathrm{Re}\left\{\left(\vec{E}_T\left(\vec{r},t\right) + \hat{z}E_z\left(\vec{r},t\right)\right)\exp\left(-i\omega t\right)\right\} \tag{1}$$

$$\vec{B}\left(\vec{r},t\right) = \mathrm{Re}\left\{\left(\vec{B}_T\left(\vec{r},t\right) + \hat{z}B_z\left(\vec{r},t\right)\right)\exp\left(-i\omega t\right)\right\} \tag{2}$$

where $\vec{E}_T$, $\vec{B}_T$ are the transverse electric and magnetic fields and E_z, B_z the longitudinal fields, which are assumed to be slowly varying of time. ω is the circular frequency.

From the Maxwell's equations (esu-Gaussian), we have

$$\frac{\partial \vec{E}_T}{\partial z} = ik_0\vec{B}_T \times \hat{z} + \nabla_T E_z \tag{3}$$

$$\frac{\partial \vec{B}_T}{\partial z} = ik_0\left(\hat{z} \times \vec{E}_T\right) + \nabla_T B_z - \frac{4\pi}{c}\hat{z} \times \vec{J}_T \tag{4}$$

$$E_z = -\frac{1}{ik_0}\nabla_T \cdot \left(\vec{B}_T \times \hat{z}\right) + \frac{4\pi}{i\omega}J_z \tag{5}$$

$$B_z = -\frac{1}{ik_0}\nabla_T \cdot \left(\hat{z} \times \vec{E}_T\right) \tag{6}$$

where $\vec{J}_T$, J_z are the transverse and longitudinal parts of current density, and $k_0 = \omega/c$ is the free space wavenumber.

The transverse components of the electromagnetic fields can be expressed as a sum over eigenmodes of the waveguide, that is

$$\vec{E}_T = \sum_{mn} V_{mn}(z,t)\,\vec{e}_{mn}(\vec{r}_T, z) \tag{7}$$

$$\vec{B}_T = \sum_{mn} I_{mn}(z,t)\,\vec{b}_{mn}(\vec{r}_T, z) \tag{8}$$

where m, n are mode numbers, V_{mn}, I_{mn} the complex voltage and current amplitudes, respectively, and $\vec{e}_{mn}$, $\vec{b}_{mn}$ the eigenvectors. The eigenvectors are defined by the following equations:

$$\nabla_T \left(\nabla_T \cdot \vec{e}'_{mn} \right) + k^2_{c,mn} \vec{e}'_{mn} = 0 \tag{9}$$

$$\left. \vec{e}_{mn} \cdot \vec{s} \right|_{onS} = 0 \tag{10}$$

for the TM modes, and

$$\nabla_T \left(\nabla_T \cdot \vec{b}''_{mn} \right) + k^2_{c,mn} \vec{b}''_{mn} = 0 \tag{11}$$

$$\left. \vec{b}''_{mn} \cdot \vec{n} \right|_{onS} = 0 \tag{12}$$

for the TE modes. The eigenfunctions are orthonormal and satisfy

$$\int e^*_{mn} \cdot e_{ml} = \begin{cases} 1 & \text{if } n = l \\ 0 & \text{if } n \neq l \end{cases} \tag{13}$$

$$\int e'^*_{mn} \cdot e''_{ml} = 0 \tag{14}$$

Here, $\vec{n}$, $\vec{s}$ are the normal and tangential unit vectors in the plane of the local cross section. S stands for the curve defining the boundary of the local cross section. $*$ represents complex conjugate.

We dot (3) with $\vec{e}^*_{mn}$ and (4) with $\vec{b}^*_{mn}$, and then integrates over the transverse cross section of the waveguide, that is

$$\iint_S \frac{\partial \vec{E}_T}{\partial z} \cdot \vec{e}^*_{mn} dS = \iint_S \left(ik_0 \vec{B}_T \times \hat{z} + \nabla_T E_z \right) \cdot \vec{e}^*_{mn} dS \tag{15}$$

$$\iint_S \frac{\partial \vec{B}_T}{\partial z} \cdot \vec{b}^*_{mn} dS = \iint_S ik_0 \left(\hat{z} \times \vec{E}_T \right) \cdot \vec{b}^*_{mn} dS + \iint_S \nabla_T B_z \cdot \vec{b}^*_{mn} dS$$

$$- \iint_S \frac{4\pi}{c} \hat{z} \times \vec{J}_T \cdot \vec{b}^*_{mn} dS \tag{16}$$

Using the orthogonal normalization of the waveguide mode eigenvectors, we get the generalized telegrapher's equations:

$$\left(1 + \frac{k_{c,mn}^2}{k_0^2}\right) \frac{\partial I_{mn}(z,t)}{c\partial t}$$

$$= ik_0 \left(1 - \frac{k_{c,mn}^2}{k_0^2}\right) I_{mn}(z,t) - \frac{\partial V_{mn}(z,t)}{\partial z} + \sum_{ml} K_{mn,ml} V_{ml}(z,t)$$

$$-S_{z,mn} + \int_C dl n \cdot e_{mn}^* \left(E_z + r_w' \vec{n} \cdot E_T\right) \tag{17}$$

$$\left(1 + \frac{k_{c,mn}^2}{k_0^2}\right) \frac{\partial V_{mn}(z,t)}{c\partial t}$$

$$= ik_0 \left(1 - \frac{k_{c,mn}^2}{k_0^2}\right) V_{mn}(z,t) - \frac{\partial I_{mn}(z,t)}{\partial z} - \sum_{ml} K_{ml,mk} I_{ml}(z,t) - S_{T,mn}$$

$$-\frac{1}{ik_0} \int_C dl \nabla_\perp \cdot b_{mn}^* \vec{n} \cdot (E_T \times \hat{z}) \tag{18}$$

where $K_{mn,ml}$ is the mode coupling term due to the varying wall radius. $S_{T,mn}$ and $S_{z,mn}$ are the coupling terms between current source and the modes. r_w' is the derivative of radius r_w to the axial variable z.
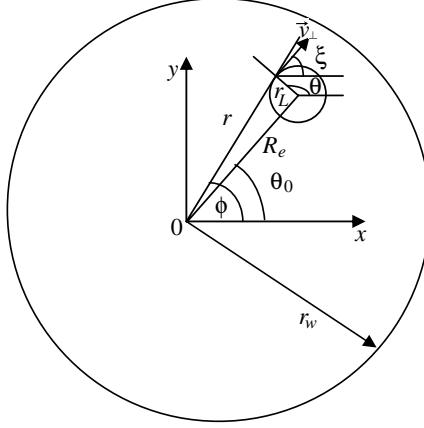
Consider the interaction of a relativistic electron beam with electromagnetic fields in the complex cavity gyrotron. The Lorenz force equation is written as

$$\frac{d(\gamma\vec{v})}{dt} = \frac{-e}{m} \left[\vec{E}(r,t) + \frac{1}{c}\vec{v} \times \left(\vec{B}(\vec{r},t) + \vec{B}_0(r,z)\right)\right] \tag{19}$$

where γ is the relativistic energy factor, $\vec{v}$ the velocity of the electron, e/m the ratio of the charge to rest mass for an electron, and $\vec{E}(\vec{r},t)$ and $\vec{B}(\vec{r},t)$ are the RF fields, $\vec{B}_0(r,z)$ is the guiding magnetic field.

Using the transformation relations of coordinates (see Figure 1), assuming that the axial magnetic field is strong and thus the Larmor radius is small and the particles essentially follow the magnetic field lines, taking axial position z as the free variable. we finally obtain the following equations under the guiding-center coordinate system:

$$\frac{\partial(\gamma\beta_\perp)}{\partial z} = \frac{1}{\beta_z} \text{Re} \left\{(\gamma\beta_\perp)^{s-1} \exp(-is\psi) \sum_{mn} (V_{mn} - \beta_z I_{mn}) F_{\perp mn,s}\right\}$$

$$+ \frac{\gamma\beta_\perp}{2} \frac{\partial \ln B_0}{\partial z} \tag{20}$$

Figure 1. A schematic diagram of the relationship between the guiding center position (R_e, θ_0) and actual position (r, ϕ) on cross section of the gyrotron.

$$\frac{\partial (\gamma \beta_z)}{\partial z} = \frac{1}{\beta_z} \text{Re} \left\{ (\gamma \beta_\perp)^s \exp\left(-is\psi\right) \sum_{mn} \left(I_{mn} - \frac{ik_0}{k_{c,mn}^2} S_{z,mn} \right) F_{\|mn,s} \right\}$$
$$- \frac{\gamma \beta_\perp^2}{2\beta_z} \frac{\partial \ln B_0}{\partial z} \tag{21}$$

$$\frac{\partial \psi}{\partial z} = \frac{1}{\gamma \beta_\perp \beta_z} \text{Im} \left\{ (\gamma \beta_\perp)^{s-1} \exp(-is\psi) \sum_{mn} (V_{mn} - \beta_z I_{mn}) F_{\perp mn,s} \right\}$$
$$+ \frac{1}{\beta_z} \left(\frac{k_0}{s} - \frac{\Omega_0}{\gamma c} \right) \tag{22}$$

$$\frac{\partial \gamma}{\partial z} = \frac{1}{\gamma \beta_z} \text{Re} \left(\begin{array}{l} \sum_{mn} V_{mn} \left[(\gamma \beta_\perp)^s \exp\left(-is\psi\right) F_{\perp mns} \right] \\ + (\gamma \beta_z) \left[\sum_{mn} \left(I'_{mn} - \frac{ik_0}{k_{c,mn}^2} S_{zmn} \right) \right. \\ \left. \left((\gamma \beta_\perp)^s \exp\left(-is\Psi\right) F'_{\|mns} \right) \right] \end{array} \right) \tag{23}$$

where V_{mn}, I_{mn} are normalized to e/mc^2, $\beta_\perp$. β_z are electrons transverse and longitudinal velocity normalized to light speed. $\Omega_0 = eB_0(z)/mc$ is the nonrelativistic cyclotron frequency. $\psi = \xi + \omega t/s + \theta_0$, s is the harmonic number. The summation is over TE and TM modes except for the longitudinal current source, which exists only for the TM modes. $F_{\perp mn,s}$, $F_{\|mn,s}$ are coupling coefficients between fields and the

electrons which are given by

$$
\begin{aligned}
&F'_{\perp mn,s} \\
&= c'_{mn} \frac{i \left(k'_{c,mn}\right)^s}{\left(\frac{\Omega_0}{c}\right)^{s-1}(2^s)(s-1)!} J_{m+s}\left(k'_{c,mn}R_e\right) \exp\left(i\left(m+2s\right)\theta_0 + is\frac{\pi}{2}\right)
\end{aligned} \tag{24}
$$

$$
\begin{aligned}
&F'_{\parallel mn,s} \\
&= c'_{mn} \frac{\left(k'_{c,mn}\right)^{s+2}}{ik_0\left(\frac{\Omega_0}{c}\right)^s 2^s (s)!} J_{m+s}\left(k'_{c,mn}R_e\right) \exp\left(i\left(m+2s\right)\theta_0 + is\frac{\pi}{2}\right)
\end{aligned} \tag{25}
$$

for TM modes with $c'_{mn} = \frac{1}{j_{mn}\sqrt{\pi}J'_m(j_{mn})}$, and

$$
F''_{\perp mn,s} = -c''_{mn}\left(\frac{\left(k_{c,mn}\right)^s}{\left(\frac{\Omega_0}{c}\right)^{s-1}(2^s)(s-1)!} J_{m+s}\left(k_{c,mn}R_e\right)\right.
$$

$$
\left. \exp\left(i\left(m+2s\right)\theta_0 + is\frac{\pi}{2}\right)\right) \tag{26}
$$

$$
F''_{\parallel mn,s} = \frac{F''_{\perp mn,s}}{\gamma} \tag{27}
$$

for the TE modes with $c''_{mn} = \frac{1}{\sqrt{\pi(j'^2_{mn}-m^2)}J_m(j'_m)}$
where R_e and θ_0 are the guiding center radius and the angle.

When the trajectories of the electrons are known, the current source $S_{T,mn}$ and $S_{z,mn}$ are calculated from current density $\vec{J}_T$ and J_z, which satisfy

$$
\vec{J}_T = \sum_i -e\delta\left(\vec{r}_\perp - r_{\perp i}\right)\delta\left(z - z_i\right)\vec{v}_{\perp i} \tag{28}
$$

$$
J_z = \sum_i -e\delta\left(\vec{r}_\perp - r_{\perp i}\right)\delta\left(z - z_i\right)v_{zi} \tag{29}
$$

Substituting (28) into $S_{T,mn}$ in (18) and (29) into $S_{z,mn}$ in (17), and then, averaging over a high-frequency period, we get

$$
S'_{z,mn} = \frac{4\omega e^2}{mc^3} \left\langle(\gamma\beta_\perp)^s \exp\left(is\psi\right)\right\rangle F'^{*}_{\parallel mn,s} \tag{30}
$$

$$
S'_{T,mn} = \frac{4\omega e^2}{mc^3} \left\langle \frac{(\gamma\beta_\perp)^s}{\gamma\beta_z} \exp\left(is\psi\right)\right\rangle F'^{*}_{\perp mn,s} \tag{31}
$$

$$
S''_{T,mn} = \frac{4\omega e^2}{mc^3} \left\langle \frac{(\gamma\beta_\perp)^s}{\gamma\beta_z} \exp\left(is\psi\right)\right\rangle F''^{*}_{\perp mn,s} \tag{32}
$$

Equations (17), (18) and (20)–(23), together with (30)–(32), constitute the self-consistent nonlinear theory model. To solve these equations, we need boundary conditions for fields and initial conditions for electrons describing initial values of the injected electron beam.

For at the left end of the open-ended gyrotron, the fields are usually evanescent and at the right end outgoing, the following boundary conditions can be adopted

$$V_{mn}(z_{in}) = 1 \qquad (33)$$

$$\left. \frac{dV_{mn}}{dz} - \gamma_{mn} V_{mn} \right|_{z=z_{in}} = 0 \qquad (34)$$

$$\left. \frac{dV_{mn}(z)}{dz} - j\beta_{mn} V_{mn}(z) \right|_{z=z_{out}} = 0 \qquad (35)$$

where $\beta_{mn}^2 = k_0^2 - k_{c,mn}^2$, $\gamma_{mn}(z_{in}) = \sqrt{k_{c,mn}^2(z_{in}) - k_0^2}$. Here, (33) represents the fields initial conditions at the left end of the interactin region, which are implemented only at the first time step. (34) (35) are the fields boundary conditions which are combined with the generalized telegrapher's equations to decide the fields amplitudes in the interaction region. These boundary conditions are performed at each time step.

The initial conditions of the electron motion are described as follows:

1) All the electrons have the same energy.
2) The initial phases are uniformly distributed. That is, the electrons are uniformly distributed over the guiding center angle θ_0 and the gyrating angle θ

$$\theta_{0j} = \frac{2\pi}{N_1}(j-1), \quad j = 1, \ldots, N_1 \qquad (36)$$

$$\theta_i = \frac{2\pi}{N_2}(i-1), \quad i = 1, \ldots, N_2 \qquad (37)$$

where N_1 is the number of electron cyclotron trajectories and N_2 the number of the particles on every electron cyclotron trajectory.

At the same time, it is assumed that N_t patches of particles are introduced into the gyrotron each wave period. That is,

$$\omega t_k = \frac{2\pi}{N_t}(k-1), \quad k = 1, \ldots, N_t \qquad (38)$$

When we show the distribution of the ωt, θ_0 and θ, according to $\psi = \xi + \omega t/s + \theta_0$, we can get the the distribution of angle ψ.

Solving the generalized telegrapher's equations for the voltage and current amplitudes, we can obtain fields at any position. The generalized telegrapher's equations are solved by the classic implicit finite-difference scheme,which are not bounded by stability conditions and relatively large time step is allowed. This method requires relatively few computing resources. Furthermore, we simplify the generalized telegrapher's equations and get a series of second-order differential equations. For each mode, the amplitudes are determined numerically by a tridiagonal matrix. We use Thomas algorithm for solving the tridiagonal equations. Then, the generalized telegrapher's equations receive solved.

The equations of motion could be obtained by fourth-order Runge-Kutta method. At each time step all particles move from the entrance plane $z = 0$ to $z = L$ (L is the length of interaction region). Using a relatively small number of particles (choose one wave period particles), we calculate the trajectories and the current source for updating the electromagnetic fields synchronously.

3. RESULTS AND ANALYSIS

Based on the above time-dependent nonlinear theory model, a calculation code is developed and a complex cavity gyrotron is simulated in detail. The schematic of the gyrotron under study is shown in Figure 2, whose dimensions and working parameters [19] are given in Table 1 and Table 2, respectively. The gyrotron is designed to operate in TE_{021}–TE_{031} modes with second harmonic at 94 GHz.

The dimension of the complex cavity gyrotron has important
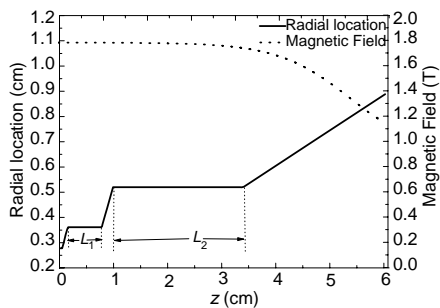
Figure 2. Configuration of the complex cavity gyrotron (solid line) and the magnetic field (dot line) under study.
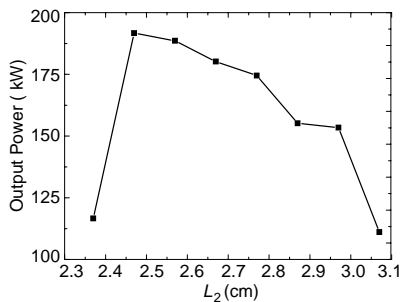
Figure 3. Curve of output power as a function of the cavity 2 length L_2.

Table 1. Complex cavity gyrotron dimensions.

Cavity 1 length	0.63 cm	Cavity 1 radius	0.36 cm
Cavity 2 length	2.47 cm	Cavity 2 radius	0.52 cm
The first taper length	0.10 cm	The first taper angle	40°
The second taper length	0.21 cm	The second taper angle	35°
Output taper length	2.62 cm	Output taper length	8°

**Table 2.** Working parameters of the complex cavity gyrotron.

Beam Voltage	50 kV	Beam Current	10 A
$\alpha\,(v_\perp/v_z)$	1.65	Magnetic Field	1.78 T
Operation Mode	TE_{021}–TE_{031}	Cyclotron Harmonic	2nd

effect on the operating mode and interaction efficiency. Especially, the output performance is strongly influenced with the length of the second cavity. The output power as a function of the cavity length L_2 is given in Figure 3. From the curve, we can get the optimal output power with proper selection of the cavity length. When the cavity length L_2 is equal to 2.47 cm, the output power is the maximum, which is about 191 kW and corresponds to about 38.3% efficiency.

By adjusting the dimension of the complex cavity gyrotron, we finally get a set of optimized parameters. The simulated gyrotron performance for several working parameters variations is given in the following Figures 4–9 with the optimal gyrotron dimensions.

There are multiple modes in the complex cavity gyrotron. In addition to TE_{021} and TE_{031}, other higher modes may be excited near the up-tapered sections such as TE_{041}. For the simulated complex cavity gyrotron is well designed and the parameters are selected to depress the unwanted modes, only the TE_{021}, TE_{031} and TE_{041} are considered in the simulation. The normalized voltage amplitudes are shown in Figure 4. One can see in the first cavity only mode TE_{021} is excited and other modes are depressed, while the second cavity mainly works in TE_{031} mode, TE_{021} and TE_{041} are restrained, which meets the design requirements.

Figure 5 shows the dependence of efficiency on axial coordinate z. In the first cavity, the electrons are prebunched for TE_{021} mode and the effect on efficiency is very small. While in the taper of the second
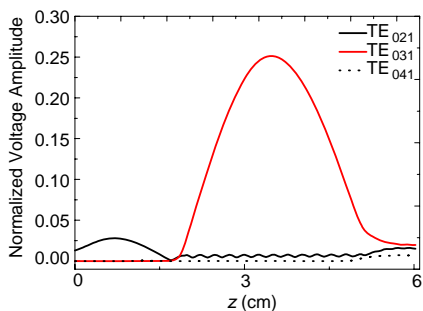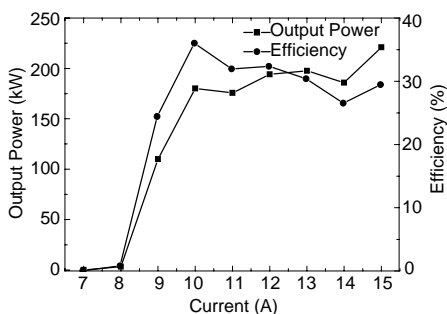
Figure 4. The normalized voltage amplitude of the operating mode TE$_{021}$–TE$_{031}$ (solid line, black line is TE$_{021}$, red line is TE$_{031}$) and higher order mode as a function of z.
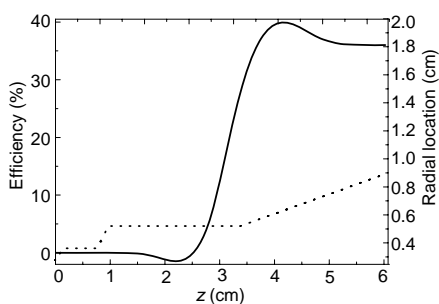
Figure 5. Efficiency as a function of the axial variable z.
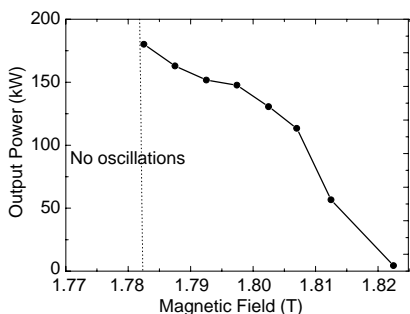
Figure 6. Dependence of output power on the axial magnetic field.

Figure 7. Output power and efficiency versus beam current.

cavity, the efficiency does not change at once. The reason is that the TE$_{031}$ mode is not completely stably coupled. The electrons are still in prebunching state, thus the efficiency could drop in the second cavity. However, as the TE$_{031}$ mode reaches steady, the efficiency is greatly improved, and reaches 36%.

A small change of magnetic field in gyrotron has a great influence on output power. Figure 6 shows dependence of output power on the axial magnetic field. The maximum output power occurs at 1.7825 T. As the magnetic field increases, the output power is sensitive to the magnetic field and decreases quickly. Since the magnetic field determines the electron cyclotron harmonic frequency, accordingly it

decides the intensity of the beam-wave interaction. Below 1.78 T, the gyrotron can not oscillate [20].

The beam current and output power are closely related. Overhigh and overlow current can not bring the greatest output power. From Figure 7, we show output power and efficiency versus beam current. As the beam current varies from 9 A to 15 A, the output power changes between 150 kW and 220 kW with the efficiency about 30%. When the beam current is less than 8 A, the gyrotron can not start oscillation. As shown in Figure 7, the complex cavity gyrotron has the optimization of the output power at current 10 A.

The output power versus beam voltage is plotted in Figure 8. Output power increases steadily with beam voltage below 50 kV. At beam voltage near 50 kV, the output power attains the maximum. Then there is a roll-off occurring at the highest voltage level. When the beam voltage is greater than 51 kV, there is no oscillations in the gyrotron. So we choose 50 kV as working voltage.
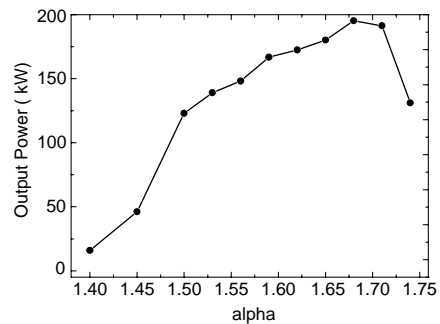
Figure 9 shows the dependence of the output power on the velocity ratio α which is defined as the ratio of transverse velocity and axial velocity. The alteration of α can cause electron beam transverse energy variance. Thus it influences the cluster circumstances and the output power.

Based on the above analysis, the optimized working parameters are obtained. In order to examine the results of the nonlinear code, MAGIC code is used to simulate this complex cavity gyrotron. Figure 10 gives the results of the MAGIC.
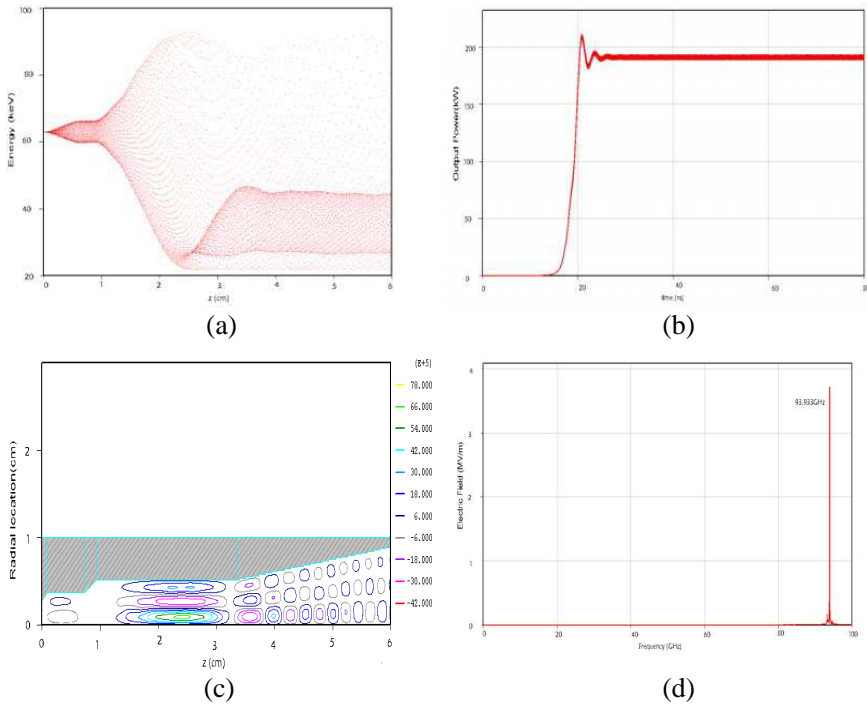
Figure 10(a) shows electrons kinetic energy as a function of z. It shows that the kinetic energy has a slight change in the first cavity, while a great change in the second cavity. The electrons have bunched
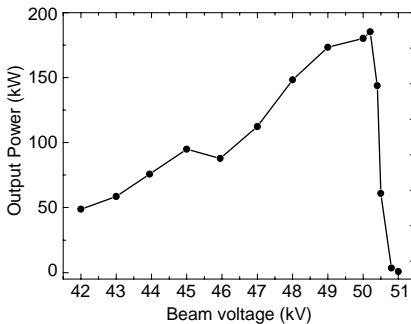
Figure 8. Output power versus beam voltage.

Figure 9. Output power as a function of the velocity ratio.

(a)

(b)

(c)

(d)

Figure 10. (a) Dependence of the electrons energy on z. (b) Output power as a function of time. (c) Distributed scheme of poloidal electric field. (d) Frequency spectrum of the electric field in the output end.

already in the second cavity and the electrons energy change indicates that there is an energy loss from the electrons. The instantaneous output power as a function of time is shown in Figure 10(b). The output power reaches steady state at 25 ns. The maximum peak output power of the MAGIC code is 192 kW, 38.4% efficiency. For comparison, the results of the nonlinear theory code is 180 kW, 36% efficiency. The two methods of the results are found to be in quite agreement. Figure 10(c) illustrates the poloidal electric field distribution. One can see that the first cavity operates in TE_{021} mode and the second cavity TE_{031} mode. This is consistent with that in Figure 4. The frequency spectrum of the electric field in the output end is given in Figure 10(d). When the driver frequency is 94 GHz, we get a frequency spectrum of 93.933 GHz and the frequency spectrum is pure.

For comparision, we get above numerical simulation results at the same computer, which is on the platform of intel xeor CPU E5430

and Window xp (64 bit) operating systems. The CPU time needed by nonlinear theory code is 5 minutes and the MAGIC code is 113 minutes. Obviously, the time needed by the nonlinear theory code is much shorter. Therefore, the nonlinear theory code can be used as a design tool.

4. CONCLUSION

A self-consistent, time-dependent nonlinear theory model is provided. A 94 GHz second harmonic complex cavity gyrotron is studied by using the nonlinear theory. The effects of various parameters, such as beam current, beam voltage, magnetic field and velocity ratio on the output power and efficiency are discussed in detail. Optimized parameters of the complex cavity gyrotron have been found. The agreement between results from the nonlinear theory model and the MAGIC code implies that the time-dependent self-consistent nonlinear theory and the corresponding code are effective for the simulation of the complex cavity gyrotron.

REFERENCES

1. Flyagin, V. A., A. V. Gaponov, M. I. Petelin, and V. K. yulpatov, "The gyrotron," *IEEE Trans. on Microwave Theory and Techniques*, Vol. 25, No. 6, 514–521, 1977.
2. Chu, K. R., "The electron cyclotron maser," *Reviews of Modern Physics*, Vol. 76, No. 2, 489–540, 2004.
3. Pavelyev, V. G. and S. E. Tsimring, "Open resonator. Inventor's certificate 616664," *Byull. Izobret.*, Vol. 17, 240, USSR, 1979.
4. Gaponov, A. V., V. A. Flyagin, A. L. Goldenberg, G. S. Nusinovich, S. E. Tsimring, V. G. Usov, and S. N. Vlasov, "Power millimeter-wave gyrotrons," *Int. J. Electronics*, Vol. 51, No. 4, 277–302, 1981.
5. Carmel, Y., K. R. Chu, M. Read, A. K. Ganguly, and D. Dialetis, "Realization of a stable and highly efficient gyrotron for controlled fusion research," *Physical Review Letters*, Vol. 50, No. 2, 112–116, 1983.
6. Pavelyev, V. G., S. E. Tsimring, and V. E. Zapevalov, "Coupled cavities with mode conversion in gyrotrons," *Int. J. Electronics*, Vol. 63, No. 3, 379–391, 1987.
7. Dumbrajs, O. and B. Jodicke, "Mode competition in a complex cavityfor gyrotrons," *International Conference on Infrared and Millimeter Waves*, 198–199, 1987.

8. Niu, X.-J., L. Wang, and H.-F. Li, "Experimental investigation of 94 GHz second-harmonic gyrotrons," *IEEE International Vacuum Electronics Conference (IVEC)*, 485–486, 2009.

9. Barker, R. J. and E. Schamiloglu, *High-power Microwave Sources and Technologies,* IEEE, Piscataway, NJ, 2001.

10. Goplen, B., L. Ludeking, D. Smithe, and G. Warren, "User configurable MAGIC code for electromagnetic PIC calculations," *Comput. Phys. Commun.*, Vol. 87, Nos. 1–2, 54–86, 1995.

11. Fliflet, A. W. and W. M. Manheimer, "Nonlinear theory of phase-locking gyrotron oscillators driven by an external signal," *Physical Review A*, Vol. 39, No. 7, 3432–3443, 1989.

12. Fliflet, A. W., R. C. Lee, S. H. Gold, W. M. Manheimer, and E. Ott, "Time-dependent multimode simulation of gyrotron oscillators," *Physical Review A*, Vol. 43, No. 11, 6166–6176, 1991.

13. Nusinovich, G. S., "Linear theory of a gyrotron in weakly tapered external magnetic field," *Int. J. Electronics*, Vol. 64, No. 1, 127–135, 1988.

14. Borie, E. and B. Jödicke, "Self-consistent theory of mode competition for gyrotrons," *Int. J. Electronics*, Vol. 72, Nos. 5–6, 721–744, 1992.

15. Vlasov, A. N. and T. M. Antonsen, "Numerical solution of fields in lossy structures using MAGY," *IEEE Trans. on Electron. Devices*, Vol. 48, No. 1, 45–55, 2001.

16. Fliflet, A. W., M. E. Read, K. R. Chu, and R. Seely, "A self-consistent field theory for gyrotron oscillators: Application to a low Q gyromonotron," *Int. J. Electronics*, Vol. 53, No. 6, 505–521, 1982.

17. Levush, B., T. M. Antonsen, Jr., A. Bromborsky, W. Lou, and Y. Carmel, "Theory of relativistic backward wave oscillator with end reflections," *IEEE Trans. Plasma Sci.*, Vol. 20, No. 3, 263–280, 1992.

18. Guo, J. H., S. Yu, X. Li, and H. F. Li, "Study on nonlinear theory and code of beam-wave interaction for gyroklystron," *J. Infrared Milli. Terahz. Waves*, Vol. 32, 1382–1393, 2011.

19. Niu, X.-J., L. Wang, and H.-F. Li, "94 GHz second-harmonic gyrotron with complex cavity," *IEEE International Vacuum Electronics Conference (IVEC)*, 469–470, 2009.

20. Aune, P., M. Fourrier, and G. Mourier, "A method for determining oscillation area in microwave tubes," *Journal of Electromagnetic Waves and Applications*, Vol. 8, No. 6, 725–742, 1994.